Experimental observation of quantum oscillation of surface chemical reactivities

Xucun Ma, Peng Jiang, Yun Qi, Jinfeng Jia, Yu Yang, Wenhui Duan, Wei-Xue Li, Xinhe Bao, S. B. Zhang, and Qi-Kun Xue

This information is current as of May 2007.

Supplementary Material	Supplementary material can be found at: www.pnas.org/cgi/content/full/0611024104/DC1 This article has been cited by other articles: www.pnas.org#otherarticles
E-mail Alerts	Receive free email alerts when new articles cite this article - sign up in the box at the top right corner of the article or click here.
Rights & Permissions	To reproduce this article in part (figures, tables) or in entirety, see: www.pnas.org/misc/rightperm.shtml
Reprints	To order reprints, see: www.pnas.org/misc/reprints.shtml

Notes:

Experimental observation of quantum oscillation of surface chemical reactivities

Xucun Ma[†], Peng Jiang[†], Yun Qi[†], Jinfeng Jia[‡], Yu Yang[‡], Wenhui Duan[‡], Wei-Xue Li[§], Xinhe Bao[§], S. B. Zhang[¶], and Qi-Kun Xue[†‡‖]

[†]Institute of Physics, Chinese Academy of Sciences, Beijing 100080, China; [‡]Department of Physics, Tsinghua University, Beijing 100084, China; [§]Dalian Institute of Chemical Physics, Chinese Academy of Sciences, Dalian 116023, China; and [¶]National Renewable Energy Laboratory, Golden, CO 80401

Here we present direct observation of a quantum reactivity with respect to the amounts of O_2 adsorbed and the rates of surface oxidation as a function of film thickness on ultrathin (2–6 nm) Pb mesas by scanning tunneling microscopy. Simultaneous spectroscopic measurements on the electronic structures reveal a quantum oscillation that originates from quantum well states of the mesas, as a generalization of the Fabry–Pérot modes of confined electron waves. We expect the quantum reactivity to be a general phenomenon for most ultrathin metal films with broad implications, such as nanostructure tuning of surface reactivities and rational design of heterogeneous catalysts.

Pb(111) | quantum size effects | scanning tunneling microscopy | surface reactivity

For a given solid, except for surface irregularities, such as steps and defects, surface reactivity is often solely determined by its crystallographic orientation. At a reduced size, however, particularly when the characteristic length scale enters the nanometer regime, the situation can change considerably from that of the bulk (1, 2). For example, in nature, Au is the most stable metal, yet a Au nanoparticle becomes chemically reactive (when the size is ≈3 nm) and can catalyze the oxidation of CO (1). Thin films are another such example where size-dependent surface chemical activities have been observed when the thickness is in the nanometer scale (3, 4). Such properties of nanostructured materials are usually attributed to quantum size effects (QSE). However, the materials used in most previous studies suffer from size fluctuation, resulting in not well defined material properties, and hence the evidences for QSE are at best qualitative (4). In the case of thin films, a far more convincing proof of QSE would be the direct observation of an oscillatory dependence of the chemical reactivities on the film thickness, which is reported here. Although bulk Pb is not a catalyst, it may function as a catalyst at the reduced size, just like Au (1). More importantly, a quantum modulation of the chemical reactivity is a general phenomenon, reflecting the QSE in the electronic states, which should not depend on any particular material.

Our Pb mesa samples were prepared on clean Si(111)-7 × 7 surfaces by the molecular beam epitaxy technique. Semiconductor silicon was chosen as the substrate to achieve the required electron confinement within the Pb mesas (5–8). Fig. 1a shows a typical scanning tunneling microscopy (STM) image of the mesas. All mesas have flat-top geometry, presumably driven by surface energy minimization, but their bottom extends laterally over several (typically 5–10) atomic steps on the Si substrates [for details of the measurement of the geometry, see supporting information (SI) Fig. 4]. For the mesa shown in Fig. 1a, seven consecutive thicknesses, 10–16 monolayers (ML), are present, as schematically shown in Fig. 1b. The high-resolution STM images (Fig. 1c and SI Fig. 4e) clearly reveal that the top surface is exclusively (111) and of a single domain, regardless of the thickness variation. Such a unique geometry enables us to simultaneously measure the electronic structure, oxygen adsorp-

tion, and oxidation of the Pb films of different thicknesses under identical experimental conditions.

Single-crystal Pb is highly resistant to oxygen (9). Appreciable oxidation takes place only at relatively high temperature (≥370 K) or at considerable oxygen coverage at room temperature, which turns out to have destroyed the geometry of the sample in Fig. 1a. To protect the wedge-shaped mesas from possible geometry damage by high-temperature annealing [a necessary step for O_2 adsorption and oxidation, as in the case of bulk Pb (9)], we have developed a two-step approach: (i) low-temperature (≈100 K) O_2 adsorption, followed by (ii) annealing at elevated temperatures to above 220 K. The method itself also proves to be a very effective way for low-temperature oxidation (SI Figs. 5 and 6).

Results and Discussion

Oscillatory Surface Reactivity. Fig. 1d shows the STM image of a mesa (which is on the same Si substrate and is nearby from the mesa shown in Fig. 1a) after exposure to 60 langmuirs (1 langmuir = 0.133 mPa·s) of oxygen at a substrate temperature of ≈100 K. The image contains four different layer thicknesses (9–12 ML). The bright spots have a typical size of ≈1.2 nm (SI Fig. 7) and are identified as chemisorbed oxygen clusters based on scanning tunneling spectroscopy (SI Fig. 8), where a strong binding of the adsorbed clusters and the surface is observed (10, 11). Because the clusters are irregular both in size and shape, their exact chemical nature is currently unknown. Despite the fact that all of the mesas are (111) oriented, here oxygen adsorption exhibits a clear thickness dependence; the areal density of the adsorbed spots on the even layers are always larger than that on the odd layers, whereas adsorption in the same layer is essentially homogeneous. Fig. 2a shows the thickness dependence of the adsorbed oxygen (averaged over 10 samples). Except for an anomaly at 17 ML, which will be discussed later, a well defined up–down oscillation with a period of 2 ML in the adsorbed oxygen coverage is immediately evident.

Remarkably, an oscillatory behavior in surface oxidation (Fig. 1 e and f) was observed when the samples were warmed up to room temperature with an additional oxygen exposure of 120 langmuirs to enhance the oxidation effect. Oscillation on thicker layers and on various mesas was also observed (SI Fig. 9). Based on the anisotropic shape and linear chain structure (SI Fig. 6g),
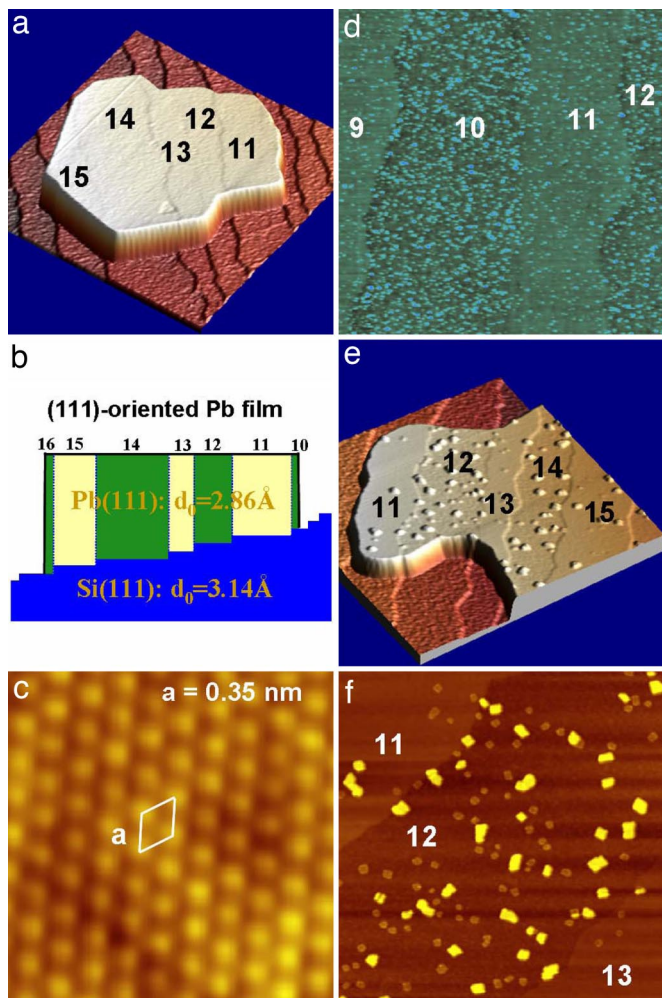
Fig. 1. Thickness-dependent oscillatory adsorption of oxygen and oxidation. (*a*) STM image (600 × 600 nm²) of a typical Pb mesa grown on the Si(111)-7 × 7 substrate, shown in a three-dimensional view. From right to left, the thickness varies from 10 to 16 ML. (*b*) Schematic drawing of the Pb mesa shown in *a*. (*c*) Atomic-resolution STM image showing that the Pb surfaces are (111)-oriented with a lattice constant of 0.35 nm. The inserted rhombus indicates the surface unit cell. This kind of image could be obtained at any part of the mesa in *a*. (*d*) STM image (339 × 339 nm²) of an oxygen-adsorbed surface after exposure to 60 langmuirs of oxygen at 100 K. (*e*) Three-dimensional STM image (500 × 500 nm²) of the oxygen-adsorbed sample in *d* after warming up to room temperature with additional oxygen exposure of 120 langmuirs. (*f*) Image (300 × 300 nm²) of the oxidized surface showing details of the monoxide at three thicknesses, 11, 12, and 13 ML (for more thicknesses, see SI Fig. 9). All images were recorded at 80 K with a tunneling current of 100 pA.
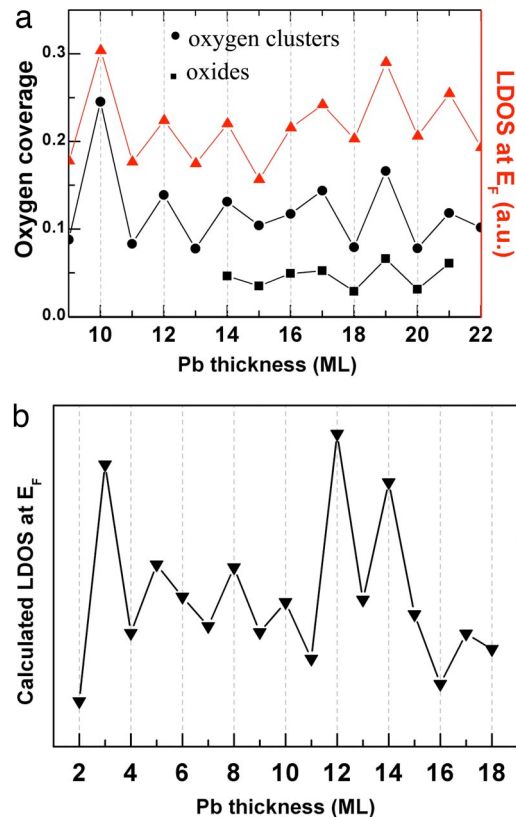

Fig. 2. Correlation between the coverage of adsorbed oxygen and the LDOS. (*a*) The measured adsorbed oxygen coverage (black dots for clusters and black squares for oxides) and the LDOS at the Fermi energy (red triangles) as a function of the Pb film thickness at 100 K. The oxygen coverage is defined as the areal density of adsorbed clusters (oxides) on the surface of Pb islands, measured as the integrated volume of these clusters (oxides) per surface unit area, assuming that the volume density of oxygen molecules is uniform and the same for different clusters. In the volume measurement by STM, a spherical shape of clusters was assumed. (*b*) The calculated LDOS at the Fermi energy as a function of the film thickness by the first-principles method. Notice that the scales of the *x* axis in *a* and *b* are different.

the yellowish rectangular islands in Fig. 1*f* and SI Fig. 9*a* are identified as massicot monoxides (PbO) (9). Variable-temperature STM experiment reveals that the adsorbed oxygen clusters are stable up to 180 K, above which the formation of the monoxide will take place (SI Figs. 6 and 10). The monoxide always develops from the previously existing oxygen clusters and grows by forming depressed holes of one monolayer deep around these clusters, suggesting that no significant diffusion of the adsorbed oxygen clusters had taken place and that only Pb atoms around the oxygen clusters were involved in the initial monoxide formation. Surprisingly, if the same amount of oxygen were exposed to the surface at room temperature, neither adsorbed oxygen nor surface oxides were observed, and the Pb surface remains its intrinsic (111)-1 × 1 structure (SI Fig. 5 *a* and *b*).

We have taken high-resolution STM images of the surfaces for

all oxygen coverages at the adsorption temperature and separately at the observation temperatures after annealing. The results indicate that localized electronic states associated with surface steps and defects (most of which are dislocations) do not play any significant role in either adsorption or oxidation. Strain is another factor to be considered, because epitaxial strain could lead to different layer spacings along the normal direction of the film. However, lattice relaxation usually takes place in the first few layers near the Pb/Si interface, whereas, near the top surface layer, spacing within the mesa is nearly the same as that of bulk Pb (12, 13). Therefore, strain effect should not contribute significantly to the reactivity variation. Furthermore, if strain is indeed important, surface oxidation should exhibit a monotonic, rather than an oscillatory, behavior with thickness. Note that, on bulk Pb(111) surfaces, such an oscillatory oxidation behavior does not exist (SI Fig. 11). It can thus be concluded that the film thickness is the deterministic factor for the variation of the surface reactivity observed here.

One may speculate that surface kinetic process such as thickness-dependent diffusion may play some important role in the oscillations. We measured the areal density of oxides as a function of thickness (the black squares in Fig. 2*a*) and found that the absolute ratio of the amounts of oxides is equal to that of the adsorbed oxygen clusters almost for any two adjacent thicknesses (except for 17 ML). For oxidation, some clusters have to diffuse
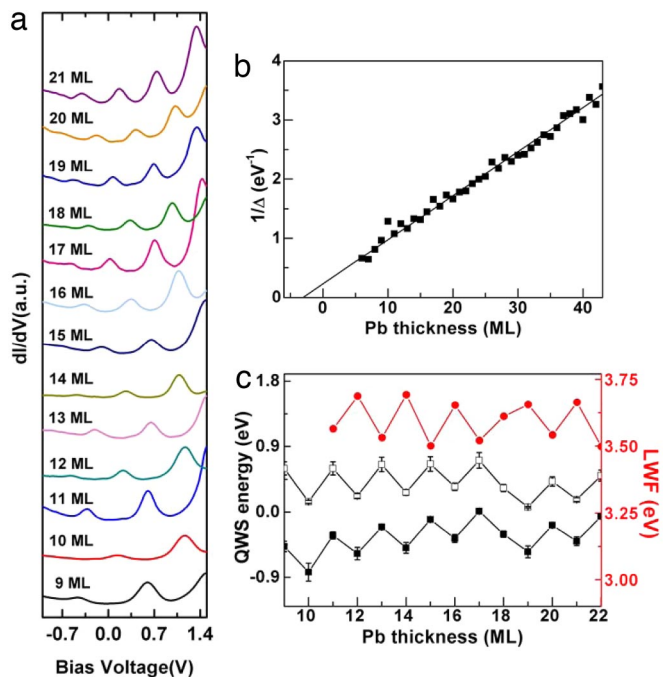
Fig. 3. Measurements of the QWS and LWF. (*a*) A series of *dI/dV* curves showing the formation of QWS in the Pb mesas. The first QWS peak below and above the Fermi energy (located at zero bias) corresponds to the HOQWS and LUQWS, respectively. (*b*) Inverse of the energy gap between HOQWS and LUQWS as a function of the Pb film thickness (from 6 to 43 ML). (*c*) The measured QWS energy (with respect to the Fermi energy) and the LWF, as a function of the film thickness. Open circles and filled squares are the LUQWS and HOQWS, respectively, whereas the red dots are the LWF.

and coalesce to form oxides, whereas some decompose and desorb from the surfaces. This observation suggests that the diffusion of oxygen species involved in oxidation should not play a significant role in the oscillating oxidation observed. We cannot rule out a possible column-crossing diffusion, but net flow of the diffusing species should be small according to this measurement. Because of different electronic structures (see Fig. 3*a*; to be discussed below), the boundary between the adjacent heights should behave like a "step." If diffusion were important, either denuded zones or preferential adsorption/reaction along the boundaries separating the even and odd layers should have been seen, as with the usual surface steps and domain boundaries, where diffusion-resulted structure decoration takes place, as is clearly observed on the single crystal Pb(111) surface in SI Fig. 11.

To examine whether this oscillation behavior is limited to oxygen, we carried out experiments with very different molecules of cobalt phthalocyanine (CoPc). The result is shown in SI Fig. 12. In this case, the thickness-dependent adsorption behavior is much more obvious. All CoPc molecules diffuse long enough and are able to reach the energetically favorable regions (10, 12, 14, 17 and 19 ML) where stronger oxygen adsorption and oxidation are always observed to form an ordered self-assembled monolayer, leaving other regions (11, 13, 15, 16, and 18 ML) intact. With this experiment, the influence thickness-dependent diffusion can safely be ruled out. Moreover, here there is no difficulty in identifying the adsorbed species; the individual CoPc molecules are clearly resolved and identified in the high-resolution STM image in SI Fig. 12*c*.

Correlation Between Surface Reactivity and QSE. The observed oscillatory reactivity can be preliminarily attributed to the QSE (3, 4). When the thickness of a metal film is comparable to the

wavelength (λ_F) of the electrons at the Fermi energy (E_F), the film can be treated as a Fabry–Pérot interferometer of the electron de Broglie waves (14). For Pb, $\lambda_F = 1.06$ nm, which is nearly 4 times of the interplanar distance d_0 along the crystallographic [111] direction. This coincidence ($\lambda_F \approx 4d_0$) suggests that, when 1 ML of Pb is added or removed, electron interference will change from being constructive to destructive and vice versa, leading to a 2-ML modulation of the electronic structure (15–19). More accurate analysis indicates that the exact period should be 1.8 ML. The small difference between 2 ML and 1.8 ML results in a 9-ML beating mode on top of the finer 2-ML oscillations. This result explains the anomaly observed at 17 ML here and in previous studies (17, 18). The great resemblance between QSE in chemical reactivity and QSE in physical transport properties (20–23) is unprecedented, suggesting a unified mechanism possibly originated from the unique behavior of the electrons at or within a small thermal energy window near the E_F.

Correlation Between Surface Reactivity and Local Density of States (LDOS). To further understand the oscillatory reactivity, we have measured the surface LDOS at the E_F [LDOS(E_F)]. The LDOS(E_F) as a function of the film thickness is shown by the red triangles in Fig. 2*a*, in which a 2-ML oscillation superimposed on a 9-ML beating envelope is clearly seen. The beating node appears at 17 ML and again at 26 ML (data not shown), in total agreement with that of the surface chemical reactivity (shown by the black dots in Fig. 2*a*).

Fig. 2*b* shows the thickness-dependent LDOS(E_F) calculated by the first-principles method. Qualitatively speaking, experiment and theory are consistent with each other: Both indicate an even/odd oscillation and the existence of a 9-ML beating mode. The influence of the electronic structure on the chemical reactivity has been studied theoretically before (24–28). According to the simplest Newns–Anderson adsorption model (25), as an oxygen molecule approaches the surface of the Pb (which can be treated as a free-electron-like metal), the anti-bonding Π^* state of the O_2 hybridizes with the sp-band of the surface such that the Π^* state broadens into a resonant state. Surface one-electron image potential will shift this resonant state down in energy to below the E_F. This downshift and subsequent filling of the Π^* state leads to dissociative adsorption. A lower LDOS(E_F) implies that the Pb film has fewer electronic states to respond, whereas a higher LDOS(E_F) implies that the film has more electronic states to respond, to the presence of the oxygen. Therefore, a higher LDOS(E_F) means a higher probability in the above hybridization process, causing the Π^* resonance to move to lower energies and to be occupied or, in other words, causing a higher surface reactivity.

Next, we discuss how the LDOS in a broader energy range would respond to the quantization of the electronic states. Fig. 3*a* shows a series of *dI/dV* curves in the energy range from −0.9 to +1.50 eV for thicknesses between 9 and 21 ML. The results here reveal clearly the formation of well defined quantum well states (QWS) in the LDOS, namely, the sharp peaks in Fig. 3*a*, at every layer thickness. This can be compared with our previous photoemission study (18, 22), in which the QWS was measured only in the normal direction to the film surface. The distinctive sharp peaks here are characteristic of the QWS at different quantum numbers. In Fig. 3*a*, the zero bias corresponds to the E_F. Thus, peaks closest to zero at negative and positive biases correspond to the highest occupied QWS (HOQWS) and lowest unoccupied QWS (LUQWS), respectively. When the film thickness increases, the LUQWS peak moves down to cross E_F and becomes occupied for every two added layers, resulting in a 2-ML oscillation. The 17-ML film is an exception for which the QWS resides right at E_F. The same was found again at 26 ML and 35 ML with a 9-ML separation, which is nothing but the long-wavelength beating mode discussed earlier. When fitting

the inverse of the energy gap (Δ) between the HOQWS and LUQWS, a good linear relationship between $1/\Delta$ and film thickness is obtained, as shown in Fig. 3*b* (5, 7).

Fig. 3*a* further shows that a 1-ML thickness change can induce an appreciable shift in the QWS energy, typically in the range of several hundreds of a millielectron volts, for example, 200 meV between 21 and 22 ML. Because of the large increase of the LDOS at the QWS peak positions, for a given total number of states, the resulting QSE modulation on the electronic structure and hence surface reactivity could be quite significant.

Correlation Between Surface Reactivity and Local Work Function (LWF). The work function, which is the minimum energy required to emit an electron from surface to vacuum, is thought to be one of the most fundamental properties for surface reactivity. Therefore, it was simultaneously measured here with the STM topographic image (29, 30). The formation of the QWS also leads to an oscillatory LWF, as shown by the red curve in Fig. 3*c*. The LWF varies in an energy range between 3.5 and 3.7 eV, with the same oscillatory behavior as the HOQWS discussed above. The closer the HOQWS is to the Fermi energy, the smaller the value of the LWF is. This result is reasonable because the LWF was measured at a negative sample bias, at which electrons tunneling from HOQWS to the tip usually dominate the current (16).

The above results suggest that an electronic state of the Pb mesa is very much confined to a region of the same thickness, such that the Fabry–Pérot interference of the electron wave can provide a characteristic fingerprint of that thickness.

As for the relationship between LWF and QWS, it comes mainly from the spatial distribution of the QWS electrons near the surface. Based on the density functional theory calculations, we find that the decay of the electronic state normal to the surface is much slower than others. For the latter, although their levels may be closer to E_F, their spatial distributions are much more localized. Because the magnitude of the electron density above the surface is decisive to the tunneling current and hence to the measurement of the LWF, the LWF is predominantly determined by states close to the Brillouin zone center with well defined QWS.

Estimation of the Quantum Adsorption Energy. In theory, the QSE could affect both surface thermodynamics and surface kinetics. In the latter case, it could result in, for example, an oscillation in the Pb adatom diffusion barrier between even and odd layers (31). In the present case of oxygen, however, because there is a fixed areal density ratio between the adsorbed oxygen at low temperature and oxide nanoparticles at high temperature for all film thicknesses, we expect the oxygen coverage shown in Fig. 1 to be a quantitative measure of the thermodynamics associated with the QSE.

How much does the QSE affect the adsorption energy? If we neglect the influence of diffusion (31), we can estimate the relative energy by using the following expression.

$$N_n = N_0\nu_0\exp(-E_a(n)/kT),\qquad [1]$$

where N_0 is the oxygen exposure, ν_0 is the adsorption prefactor (assumed to be a constant for all of the thicknesses), $E_a(n)$ is the activation energy at the nth layer, k is the Boltzmann constant, and $T = 100$ K is the substrate temperature. From the measured adsorption coverage (N_n) in Fig. 2, we obtained an energy difference of 9 meV between E_a ($n = 10$) and E_a ($n = 11$) for the clusters. From application point of view, a 9-meV change is significant, because it implies that a 1-ML change in the film thickness is equivalent to a temperature change of 100°.

Conclusion

By synthesizing flat-top Pb mesas on a Si(111) substrate, we unambiguously demonstrated the oscillatory surface reactivity due to the quantum size effect by using a two-step oxygen adsorption/annealing method. Our in-depth study provides quantitative accounts of the correlations between the quantum surface reactivity, the QSE, the surface LDOS, and the LWF. We expect the quantum surface reactivity to be a general phenomenon beyond just Pb and, hence, to have broad applications, such as modifying the surface chemistry of metals and to serve as a guide to nanotailoring metal catalysts.

Materials and Methods

Sample Preparation. The experiments were performed in a Unisoku ultrahigh vacuum low-temperature STM system with a molecular beam epitaxy chamber for *in situ* preparation of thin films. The base pressure of the system is better than 2.0×10^{-10} torr (1 torr = 133 Pa). Lead with a purity of 99.999% was evaporated at a flux rate of 0.32 ML/min from a PBN Knudsen cell onto clean Si(111)-7 $\times$ 7 reconstructed substrates in the molecular beam epitaxy chamber. During the Pb evaporation, the Si substrates were cooled down to 200 K by liquid nitrogen to obtain the wedge-shaped Pb mesas. The nominal thickness of the Pb layer is $\approx$4 ML, which is below the critical thickness of 10 ML to form atomically uniform films (22). After growth, the samples were transferred to the STM chamber for low-temperature STM observation. All STM topographic images were recorded at 80 K with a constant current of 100 pA. Oxygen adsorption was performed in the molecular beam epitaxy chamber by using a leak valve. During the adsorption, the oxygen pressure was kept at 2×10^{-7} torr, and the temperature of the samples was at $\approx$100 K.

Scanning Tunneling Spectroscopy and LWF Measurements. Surface LDOS and work function were measured by scanning tunneling spectroscopy at 80 K in a constant current mode (100 pA) with a lock-in technique for the clean surfaces (without oxygen exposure). The LDOS was obtained under the conditions of small bias voltage ($<$10 mV) and small modulation (5 mV) by taking the first derivative of the tunneling current with respect to the bias voltage in spectroscopic form of both dI/dV curves (at given spatial positions) and a real-space map (at a given energy). The LWF measurements were performed by modulating the tip-sample distance to collect the $d(\ln I)/dZ$ signal (29).

First-Principles Calculations. The calculations were performed by using the Vienna *ab initio* Simulation Package (VASP) (32), in which we used the density functional theory, Vanderbilt ultrasoft pseudopotentials (33), and the PW91 exchange-correlation potential (34) within the generalized gradient approximation (35). The plane-wave cutoff energy was 144 eV. Integration over the Brillouin zone was done by using the Monkhorst–Pack scheme (36) with a 21 $\times$ 21 $\times$ 1 mesh for atomic relaxations and a 41 $\times$ 41 $\times$ 1 mesh for the electronic structure. The Pb films were modeled by periodic slabs consisting of 2–18 ML, separated by a vacuum layer of 13 Å. Our theoretically lattice constant for bulk Pb was 5.028 Å, which is in good agreement with the experimental value of 4.95 Å to within 1.6%.

1. Valden M, Lai X, Goodman DW (1998) *Science* 281:1647–1650.
2. Rolison DR (2003) *Science* 299:1698–1701.
3. Danese AG, Curti FG, Bartynski RA (2004) *Phys Rev B* 70:165420.
4. Aballe L, Barinov A, Locatelli A, Heun S, Kiskinova M (2004) *Phys Rev Lett* 93:196103.
5. Altfeder IB, Matveev KA, Chen DM (1997) *Phys Rev Lett* 78:2815–2818.

CHEMISTRY

6. Budde K, Abram E, Yeh V, Tringides MC (2000) *Phys Rev B* 61:R10602–R10605.
7. Su WB, Chang SH, Jian WB, Chang CS, Chen LJ, Tsong TT (2001) *Phys Rev Lett* 86:5116–5119.
8. Menzel A, Kammler M, Conrad EH, Yeh V, Hupalo M, Tringides MC (2003) *Phys Rev B* 67:165314.
9. Thürmer K, Williams E, Reutt-Robery J (2002) *Science* 297:2033–2035.
10. King DA, Wells MG (1974) *Proc R Soc London Ser A* 339:245–269.
11. Zhukov V, Popova I, Yates JT, Jr (1999) *Surf Sci* 441:251–264.
12. Materzanini G, Saalfrank P, Lindan PJD (2001) *Phys Rev B* 63:235405.
13. Jia Y, Wu B, Weitering HH, Zhang Z (2006) *Phys Rev B* 74:035433.
14. Paggel JJ, Miller T, Chiang TC (1999) *Science* 283:1709–1711.
15. Mans A, Dil JH, Ettema ARHF, Weitering HH (2002) *Phys Rev B* 66:195410.
16. Hupalo M, Tringides MC (2002) *Phys Rev B* 65:115406.
17. Czoschke P, Hong H, Basile L, Chiang TC (2004) *Phys Rev Lett* 93:036103.
18. Zhang YF, Jia JF, Tang Z, Han TZ, Shen QT, Guo Y, Qiu ZQ, Xue QK (2005) *Phys Rev Lett* 95:096802.
19. Czoschke P, Hong H, Basile L, Chiang TC (2005) *Phys Rev B* 72:075402.
20. Jałochowski M, Bauer E, Knoppe H, Lilienkamp G (1992) *Phys Rev B* 45:13607–13613.
21. Vilfan I, Henzler M, Pfennigstorf Q, Pfnür H (2002) *Phys Rev B* 66:241306.
22. Guo Y, Zhang YF, Bao XY, Han TZ, Tang Z, Zhang LX, Zhu WG, Wang EG, Niu Q, Qiu ZQ, *et al.* (2004) *Science* 306:1915–1917.
23. Eom D, Qin S, Chou MY, Shih CK (2006) *Phys Rev Lett* 96:027005.
24. Newns DM (1969) *Phys Rev* 178:1123–1135.
25. Nørskov JK (1990) *Rep Prog Phys* 53:1253–1295.
26. Cohen MH, Ganduglia-Pirovano MV, Kudrnovský J (1994) *Phys Rev Lett* 72:3222–3225.
27. Wilke S, Cohen MH, Scheffler M (1996) *Phys Rev Lett* 77:1560–1563.
28. Binggeli N, Altarelli M (2006) *Phys Rev Lett* 96:036805.
29. Jia JF, Inoue K, Hasegawa Y, Yang WS, Sakurai T (1998) *Phys Rev B* 58:1193–1196.
30. Qi Y, Ma XC, Jiang P, Ji SH, Fu YS, Jia JF, Xue QK, Zhang SB (2007) *Appl Phys Lett* 90:013109.
31. Chan TL, Wang CZ, Hupalo M, Tringides MC, Ho KM (2006) *Phys Rev Lett* 96:226102.
32. Kresse G, Hafner J (1993) *Phys Rev B* 47:558–561.
33. Vanderbilt D (1990) *Phys Rev B* 41:R7892–R7895.
34. Perdew JP, Chevary JA, Vosko SH, Jackson KA, Pederson MR, Singh DJ, Fiolhais C (1992) *Phys Rev B* 46:6671–6687.
35. Perdew JP, Burke K, Ernzerhof M (1996) *Phys Rev Lett* 77:3865–3868.
36. Monkhorst HJ, Pack JD (1976) *Phys Rev B* 13:5188–5192.